Materials and Design 191 (2020) 108594

Contents lists available at ScienceDirect

Materials and Design

journal homepage: www.elsevier.com/locate/matdes

Conductive hybrid filaments of carbon nanotubes, chitin nanocrystals and cellulose nanofibers formed by interfacial nanoparticle complexation

Kaitao Zhang [a], Lukas Ketterle [b], Topias Järvinen [c], Shu Hong [d,a], Henrikki Liimatainen [a,*]

[a] Fiber and Particle Engineering Research Unit, University of Oulu, P.O. Box 4300, FI-90014, Finland
[b] Institute for Mechanical Process Engineering and Mechanics, Faculty of Chemical and Process Engineering, Karlsruhe Institute of Technology, 76344 Eggenstein-Leopoldshafen, Germany
[c] Microelectronics Research Unit, Faculty of Information Technology and Electrical Engineering, University of Oulu, P.O. Box 4300, FI-90014, Finland
[d] College of Materials Science and Engineering, Nanjing Forestry University, Nanjing 210037, China

HIGHLIGHTS

- Interfacial nanoparticle complexation was employed to draw filament.
- Bio-based filaments were prepared using cationic chitin nanocrystal and anionic naoncellulose as raw materials.
- The influence of drawing speed on the tensile strength was investigated.
- Conductive filament with single walled carbon nanotubes was fabricated using interfacial nanoparticle complexation.

GRAPHICAL ABSTRACT

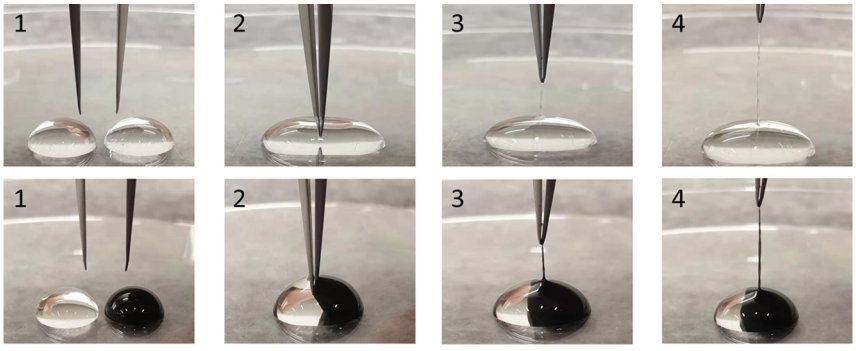

ARTICLE INFO

Article history:
Received 6 January 2020
Received in revised form 19 February 2020
Accepted 20 February 2020
Available online 21 February 2020

Keywords:
Nanocellulose
Nanochitin
Filament
Carbon nanotube
Cellulose nanofibrils
Complexation

ABSTRACT

In this paper, anionic TEMPO-oxidized cellulose nanofibers (TO-CNFs) and cationic, partially deacetylated, chitin nanocrystals (ChNCs) were used to fabricate continuous composite filaments (TO-CNF/ChNC filament) with a straightforward and sustainable aqueous process based on the interfacial nanoparticle complexation (INC) of oppositely charged nano-constituents. In particular, the role of TO-CNF and ChNC concentrations in filament drawing and the effect of drawing speed on the mechanical properties of composite filaments were investigated. Moreover, conductive filaments were fabricated by mixing single walled carbon nanotubes (SWCNTs) with TO-CNF dispersion and further complexing with the ChNC aqueous suspension. A conductive filament with an electrical conductivity of 2056 S/m was obtained. However, the increase in the SWCNTs content reduced the mechanical properties of the formed filament compared to neat TO-CNF/ChNC filament. This study not only introduces a new nanoparticle candidate to prepare filaments based on INC method but also provides potential advanced and alternative green filament to be used as wearable electronics in biomedical area.

1. Introduction

Polysaccharides are carbohydrates formed by monosaccharide condensation via hemi-acetal or hemi-ketal linkages [1]. Cellulose and

* Corresponding author.
E-mail addresses: kaitao.zhang@oulu.fi (K. Zhang), topias.jarvinen@oulu.fi (T. Järvinen), henrikki.liimatainen@oulu.fi (H. Liimatainen).

https://doi.org/10.1016/j.matdes.2020.108594

chitin are typical polysaccharides found abundantly in nature that act as structural building blocks to provide physical support to the living bodies of green plants and some marine animals. Due to the abundance, sustainability, biodegradability and low cost of many polysaccharides, interest in developing bio-based products to substitute materials based on petrochemistry has grown [2].

Cellulose, as the most abundant natural polymer on the earth, is one of the most important polysaccharides. Native cellulose is mainly found in cell walls of cellulose resources including wood, plants, tunicates, and algae [3]. With appropriate chemical [4–8], mechanical [9,10] or enzymatic treatment [11], nanocellulose (NC) with one dimension of less than 100 nm, can be extracted. Similarly, chitin, as the second most abundant polysaccharide after cellulose, is known as a cellulose analogue consisting of repeating *N*-acetylglucosamine units. It exists widely in the exoskeletons of shellfish and insects and the cell walls of fungi [12,13]. Nanosized chitin, called nanochitin (NCh), can be fabricated by disintegrating the hierarchical structure of chitin through, for example, acid hydrolysis or mechanical treatments [14–18]. Both NC and NCh have attracted notable attention, as they combine important polysaccharide properties with the unique and appealing characteristics of nanomaterials [19] such as their high aspect ratios, large surface areas, and easy surface modifications [20–22]. The outstanding physical and chemical properties of NC and NCh enable their use in a range of applications including polymer composites, emulsifiers, package materials, water treatment additives and drug delivery agents [23–27].

Cellulose and chitin exist inherently as part of composite structures formed by various biopolymers and compounds that organize in a hierarchical design with diverse functionalities [28]. Inspired by these composite architectures, various types of sustainable structural materials, such as films, hydrogels, aerogel, and filaments, have been fabricated based on the nanostructured NC and NCh [29–40]. Particularly, the composite film, hydrogel, and aerogel of NC and NCh were fabricated by the utilization of ionic interaction between anionic NC and cationic NCh [41–45]. Recently, NC-derived filaments created by the interfacial polyelectrolyte complexation (IPC) were reported based on the mechanical drawing of anionic NC and cationic chitosan [46,47]. The spinning method using IPC technique is based on the spontaneous formation of the interface complex film between two oppositely charged polyelectrolytes solutions. Self-assembled continuous filament could be obtained by pulling up the formed interface complex film [46]. This process is carried out under aqueous, neutral pH, and ambient temperature conditions, it compares favorably to many other fiber spinning processes that typically requires the use of volatile organic solvents or polymer melt [48]. Since the discovery of IPC method, various IPC fibers have been fabricated based on different combinations of oppositely charged polyelectrolytes. Besides, the biocompatible nature of IPC fiber makes them useful for a variety of applications especially in biomedical area such as drug delivery, cell culture and biosensor [48–50]. Inspired by this, we produced NC based filaments using only charged colloidal NC without any soluble polyelectrolytes, which was termed as “interfacial nanoparticle complexation (INC)” [51]. In nature, chitin is reported to present amino groups at C2 on the nanofibril surfaces, these amine groups can be protonated under acidic conditions to make chitin positively charged. Thus, it could be assumed that the spinning of positively charged NCh with negatively charged NC by INC method is also possible [52]. To our best knowledge, the filaments based on NC and NCh nanoparticles using the INC method have not yet been reported.

Carbon nanotubes (CNTs), i.e. single and multi-walled carbon nanotubes (SWCNTs and MWCNTs, respectively), have excellent physical properties as well as good electrical conductivity. They are considered promising constituents in conductive composite materials and electrochemical devices. However, their exploitation in composites requires that they are homogeneously dispersed in the matrix. It was reported early that stable hybrid dispersion was formed by the dispersion of CNT in aqueous NC suspension [53–55]. This approach was used as an efficient technique for the fabrication of NC-CNT composites, such as films [56], aerogels [57,58], hydrogels [59], and microfibers [60–62] for applications in supercapacitors, textile sensor, and so on. In particular, hybrid filaments of CNTs and NC have been prepared based on wet-spinning and 3D printing [55,60,61].

Herein, partially deacetylated chitin nanocrystals (ChNCs) were produced and used as a cationic component to engineer new type of nanocomposite filaments with anionic cellulose nanofibers (CNFs). Furthermore, conductive ChNC/CNF composite filaments were successfully designed by incorporating SWCNTs into the filaments. These green and conductive filaments can potentially be used as wearable electronic devices (such as sensors and supercapacitors) applied in biomedical area [60,62].

2. Experimental

2.1. Materials

Bleached birch (*Betula pendula*) chemical wood pulp obtained in dry sheets was used as a cellulose raw material after disintegration in deionized water. 2,2,6,6-Tetramethylpiperidinyl-1-oxy radical (TEMPO), sodium bromide (NaBr), sodium hypochlorite solution (NaClO, 15 wt%), and chitin powder from crab shells were obtained from Sigma–Aldrich (Finland). The TEMPO-oxidized CNFs (TO-CNFs) were prepared according to the previously reported method [63]. The dose of NaClO during oxidation was 10.0 mmol/g of pulp. The oxidized pulp was furtherly disintegrated via probe sonication for 1 h (Heilscher UP 400s, power discharge 0.5 s and pause 0.5 s, 60% amplitude and 22 mm probe tip diameter) to obtain the TO-CNFs. The carboxylated group content of the TO-CNFs was determined to be 1.57 mmol/g using conductometric titration method [64]. SWCNTs (Product TNST) were purchased from TimeNano (Chengdu, China). The morphological characteristics of the TO-CNF and SWCNTs are shown in Fig. S1 and S2, respectively. The dimension of the obtained TO-CNF is 172 to 958 nm in length and 5 ± 2 in width; SWCNTs aggregate into bundles (ropes) with a width of 17 ± 3 nm and individual SWNCT shows a diameter of about 1 nm.

2.2. Preparation of cationic chitin nanocrystals

Chitin surface deacetylation was conducted according to the previously reported procedure [65]. Chitin powder was suspended in aqueous NaOH (20 wt%) and refluxed for 6 h. The deacetylated chitin slurry was collected by filtration, and washed thoroughly with distilled water by centrifugation. The wet sample was dispersed in water at 1 wt %, and acetic acid was added to adjust the pH value to 4. The dispersion was passed once through a microfluidizer (Microfluidics M-110EH-30, USA) with a pair of chambers (400 and 200 μm). Then, the obtained gel-like suspension was diluted to 0.6 wt% and further disintegrated with an ultrasonicator (output power of 400 W, 13 mm probe tip diameter, 60%) for 1 h.

2.3. Preparation of TO-CNF/ChNC and SWCNTs@TO-CNF/ChNC hybrid filaments

The TO-CNF/ChNC filaments were fabricated using our previously reported INC method [51]. Aqueous ChNCs and TO-CNFs suspensions with different concentrations (from 0.15 to 0.5 wt%) were used. A drop (100 μL) of ChNC suspension was placed on a Petri dish next to a drop (100 μL) of anionic TO-CNF suspensions. A pair of tweezers was used to bring the two droplets together and draw TO-CNF/ChNC hybrid filaments using a universal testing machine. For the SWCNT containing TO-CNF/ChNC hybrid filaments, various amounts of SWCNTs powder were first mixed with 15 mL of a 0.3 wt% TO-CNF aqueous suspension and further treated with an ultrasonic homogenizer for 20 min (Heilscher UP 400s, power discharge 0.5 s and pause 0.5 s, 60% amplitude and 7 mm probe tip diameter), resulting in 0.3 wt% TO-CNF

suspension containing 0.05, 0.1, and 0.2 wt% SWCNTs, respectively. The obtained suspensions were directly used as a negatively charged component to draw the filaments with 0.3% cationic ChNC suspension. All the TO-CNF/ChNC filament containing SWCNT (SWCNT@TO-CNF/ChNC filaments) were drawn using a universal testing machine with a speed of 40 mm/min. The fresh drawn filaments were attached to a glass rod and air-dried at room temperature.

2.4. Characterization

2.4.1. Transmission electron microscopy

The morphological features of ChNCs were analyzed using a transmission electron microscope (TEM, JEOL JEM-2200FS, Japan). A small droplet of 0.005 wt% ChNC suspension was dosed on the top of a carbon-coated copper grid. After drying, the sample was negatively stained with uranyl acetate (2% w/v) for 20 min. The staining agent was removed by a small piece of filter paper and the samples were allowed to dry at room temperature. Standard conditions with 200 kV were used during the TEM analysis. The dimensions of the ChNCs were measured using iTEM (Olympus Soft Imaging Solutions GMBH, Munster, Germany) image analysis software.

2.4.2. Field emission scanning electron microscope (FESEM)

The FESEM images of the composite filaments were obtained using a field emission scanning electron microscope (FESEM, Zeiss Sigma HD VP, Oberkochen, Germany) at 0.5 kV acceleration voltage. All samples were sputtered with platinum before observation.

2.4.3. Elemental analysis

The composition of the filaments in terms of their ChNC content was calculated directly from the nitrogen content of the ChNC and formed filaments as determined using a PerkinElmer CHNS/O 2400 Series II elemental analyzer:

$$\text{ChNC in filament } [\%] = \frac{\text{N } [\%] \text{ of filament}}{\text{N } [\%] \text{of ChNC}}$$

2.4.4. Polyelectrolyte titration

The charge density of the ChNC was measured using a particle charge detector (Mütek PCD 03, USA), in which 10 mL 0.01 wt% ChNCs suspension was titrated with polyethylene sulfonate sodium (PES-Na, 1 meq/L) and the charge density was calculated based on the consumption of PES-Na [66].

2.4.5. Diffuse reflectance infrared Fourier transform spectroscopy

The chemical characterizations of the chitin, ChNC, TO-CNF, and formed composite filaments were carried out using diffuse reflectance infrared Fourier transform (DRIFT) spectroscopy. The spectra were recorded on a Bruker Vertex 80v spectrometer (USA) in the 800–4000 cm^{-1} range with 2 cm^{-1} resolution.

2.4.6. Thermogravimetric analysis

The thermogravimetric analysis (TGA) was performed using a thermal analyzer Netzsch STA 449 F3 apparatus (Germany) under nitrogen flow with a constant rate of 60 mL min^{-1}. Each measurement was heated from 30 to 700 °C at a scanning rate of 10 K/min.

2.4.7. Mechanical properties

The mechanical properties of the filaments were studied using a universal testing machine (Zwick D0724587, Switzerland) equipped with a 200 N load cell. The samples were glued on paper frames before being tested to avoid sample slippage and were then mounted onto the clamps. Once the frame was secured, the paper was cut, leaving the fiber ready for testing. All the samples were tested at a speed of 5 mm/min at room temperature and a gauge length of 20 mm using a pre-force of 0.01 N until breakage. Five replicates for each material were tested and all samples were placed at a relative humidity of 50% and a temperature of 22 °C for at least one day prior to the testing. The diameters of the filaments were measured using an optical microscope (Leica MZ6 equipped with a Leica DFC420 camera) and the cross-section was assumed to be circular. The average values and standard deviations of the diameter, tensile strength and strain were also reported.

2.4.8. Electrical conductivity measurement

The electrical conductivities of the SWCNTs@TO-CNF/ChNC filaments were measured using a two-point probe setup (Keithley 2636A SourceMeter, 21 oC, 30% relative humidity). When calculating the conductivity, the filament was regarded as a perfect round shape. At least five filaments of each kind were measured and each filament was measured two times.

3. Results and discussion

3.1. Characterization of ChNCs

The ChNCs were prepared by the partial deacetylation of α-chitin followed by microfluidic and ultrasonic disintegration. Fig. 1 shows the TEM image and the length and width distribution of the obtained ChNCs. The ChNCs displayed rod-like shapes with an average of 122 ± 44 nm in length and 6.1 ± 2.5 nm in width. The cationic charge density of the ChNCs was determined via polyelectrolyte titration to be 1.7 mmol/g.

3.2. Fabrication of TO-CNF/ChNC composite filaments

Aqueous ChNC and TO-CNF suspensions with different concentrations were used to investigate their feasibility in the composite filament drawing based on the INC. All the experiments were performed at a drawing speed of 40 mm/min using a universal testing machine. The formed filaments from various concentration pairs were dried at room temperature, and filaments with lengths of more than 200 cm were regarded as a successful drawing process. The maximum filament length in the drawing tests was limited to 693 mm because of the experimental setup.

The results of the filament drawing tests are shown in Table 1. The filaments could be formed with all the combination pairs of TO-CNF and ChNC, but the lengths of the filaments drawn by 0.5 wt% TO-CNF were less than 200 mm, indicating an unstable spinning process. This result could be ascribed to the high viscosity of 0.5 wt% TO-CNF (the viscosities of TO-CNF and ChNC could be found in Fig. S3), which may hinder the diffusion and replenishment of the consumed TO-CNF in the suspension at the complexation interface. In contrast, with lower concentration of TO-CNF, all the filaments could be drawn successfully (with filament lengths of longer than 200 mm). However, the concentration of 0.15 wt% ChNC seemed be too low for effective filament fabrication, and a maximum filament length of 450 mm was obtained. It was observed that the combination of 0.3 wt% TO-CNF with 0.3 wt% ChNC showed the best fiber drawing feasibility. All filaments for further measurements were made from 0.3 wt% TO-CNF and 0.3 wt% ChNC composition. Reason to select this combination is the good feasibility at relatively high concentration and low viscosity for TO-CNFs and ChNC.

3.3. Effect of drawing speed on the mechanical properties of TO-CNF/ChNC composite filaments

Drawing speed is one of the key factors that affects the formation of INC filaments [48]. To evaluate the influence of the drawing speed on the mechanical properties of the formed TO-CNF/ChNC filaments, different drawing speeds ranging from 40 mm/min to 500 mm/min were tested. Fig. 2 shows typical stress-strain curves, average ultimate tensile

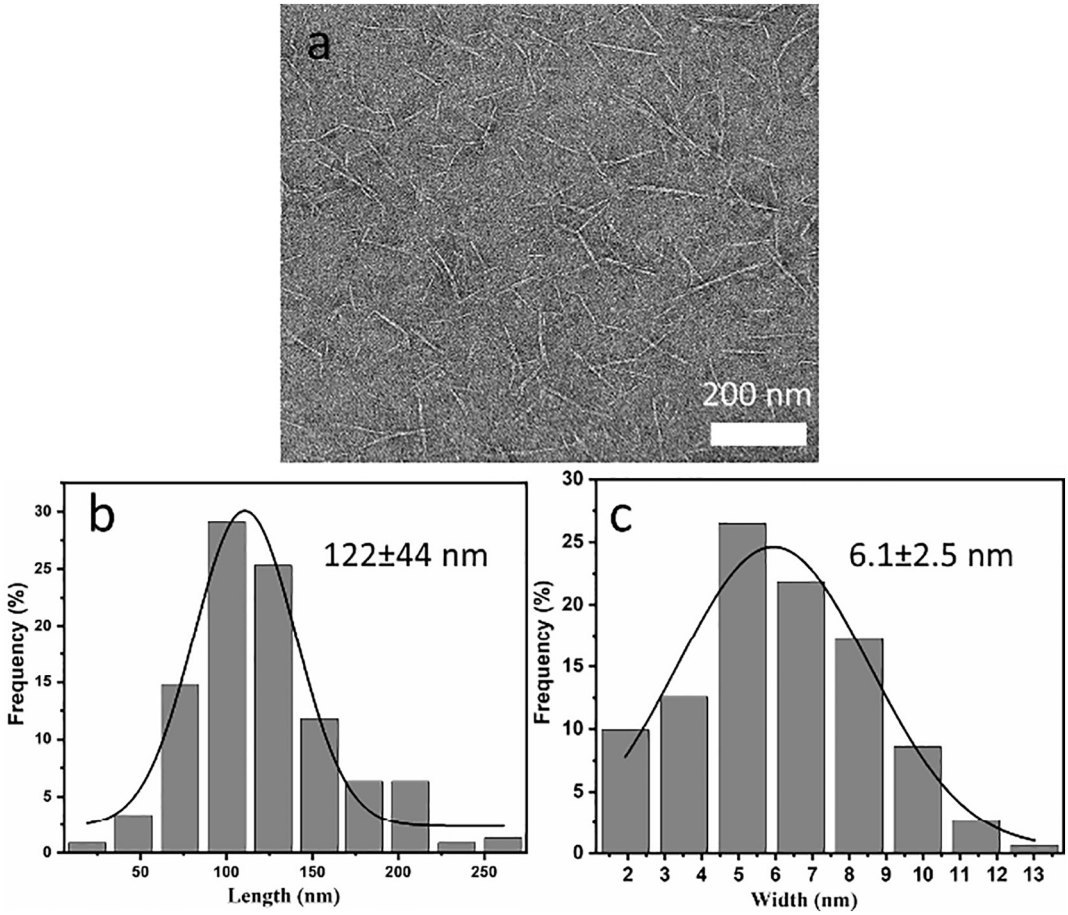

Fig. 1. TEM image (a) of the chitin nanocrystals and their length (b) and width (c) distributions.

strength, strain and Young's modulus of the formed TO-CNF/ChNC filaments with different drawing speeds. The diameter slightly decreased with increasing the drawing speed (from ~24 to 20 μm, Table S1).

The tensile strength and Young's modulus of the TO-CNF/ChNC filaments formed by the lowest speed of 40 mm/min were about 184 MPa and 8.3 GPa, respectively. The increase in the drawing speed to 100 mm/min and 150 mm/min, decreased the tensile strength and Young's modulus only slightly. At 200 mm/min, the ultimate tensile strength reached the maximum value of 188 MPa, presumably because of the improved alignment of the nanoconstituents. However, a further increase in the drawing speed dropped the ultimate tensile strength significantly. This result can be attributed to kinetics of the complexation process; in other words, too short interaction time resulted in only a partial complexation process at higher drawing speeds [48]. On the other hand, the replacement of the charged nanoparticles at the interface through diffusion and convection also requires slow drawing speed to create a stable and homogeneous filaments. With a drawing speed of 500 mm/min or higher, gel droplets were reported to appear along the longitudinal axes of the filaments because of the release of counterions and water during complexation [67]. After drying, the droplets can create irregular protuberances, which make the filament uneven and influence the mechanical properties of the formed filaments. The strain of the filaments was similar at all drawing speeds except the highest speed.

Table 1
The feasibility and lengths (mm) of the filament spinning from different combination pairs of ChNC and TO-CNF suspensions.

Sample	0.5 wt% TO-CNF	0.3 wt% TO-CNF	0.15 wt% TO-CNF
0.5 wt% ChNC	No (160)	Yes (620)	Yes (693)
0.3 wt% ChNC	No (199)	Yes (693)	Yes (693)
0.15 wt% ChNC	No (190)	Yes (333)	Yes (450)

3.4. Chemical structure of TO-CNF/ChNC filaments

The DRIFT spectra of the TO-CNF, ChNC and TO-CNF/ChNC filaments are presented in Fig. 3. TO-CNF showed the characteristic vibration bands of cellulose sample at 3490 (O—H stretching), 2900 (C—H stretching), 1170 (asymmetrical stretching vibration of C—O—C glycoside bonds) and 1123 cm^{-1} (—C—O stretching vibration of ether groups). Two typical bands at around 1623 and 1427 cm^{-1}, corresponding to the antisymmetric and C═O stretching of the carboxylate groups (COO—) formed by TEMPO oxidation, were noted [68]. The spectrum of the ChNC showed a strong and broad band centered at about 3484 cm^{-1} with a shoulder at 3269 cm^{-1}, which resulted from the overlapping of the O—H and N—H stretching vibrations of the functional groups engaged in hydrogen bonds [69]. Two characteristic bands of the amide groups at 1664 and 1580 cm^{-1} were attributed to the C═O stretching of amide I and the N—H bending vibration of the amide II, respectively [18]. Absorption bands at 2879, 1320 and 1260 cm^{-1} were attributed to symmetric and antisymmetric CH_2 vibrations of the carbohydrate ring [70]. The TO-CNF/ChNC filament exhibited a characteristic spectrum, different from those of the individual components, especially in 1800–1400 cm^{-1} the area. The bands in the TO-CNF at 1423 (symmetric stretching vibration of the carboxylate group) and 1623 cm^{-1} shifted to 1411 and 1630 cm^{-1}, respectively. Moreover, the absorption band at 1630 cm^{-1} might also belonged to the antisymmetric N—H deformation vibration in protonated amines, which has been reported in the polyelectrolyte complexes of chitosan with alginate [71] or carboxymethyl cellulose [72]. The N—H bending vibration of amides II

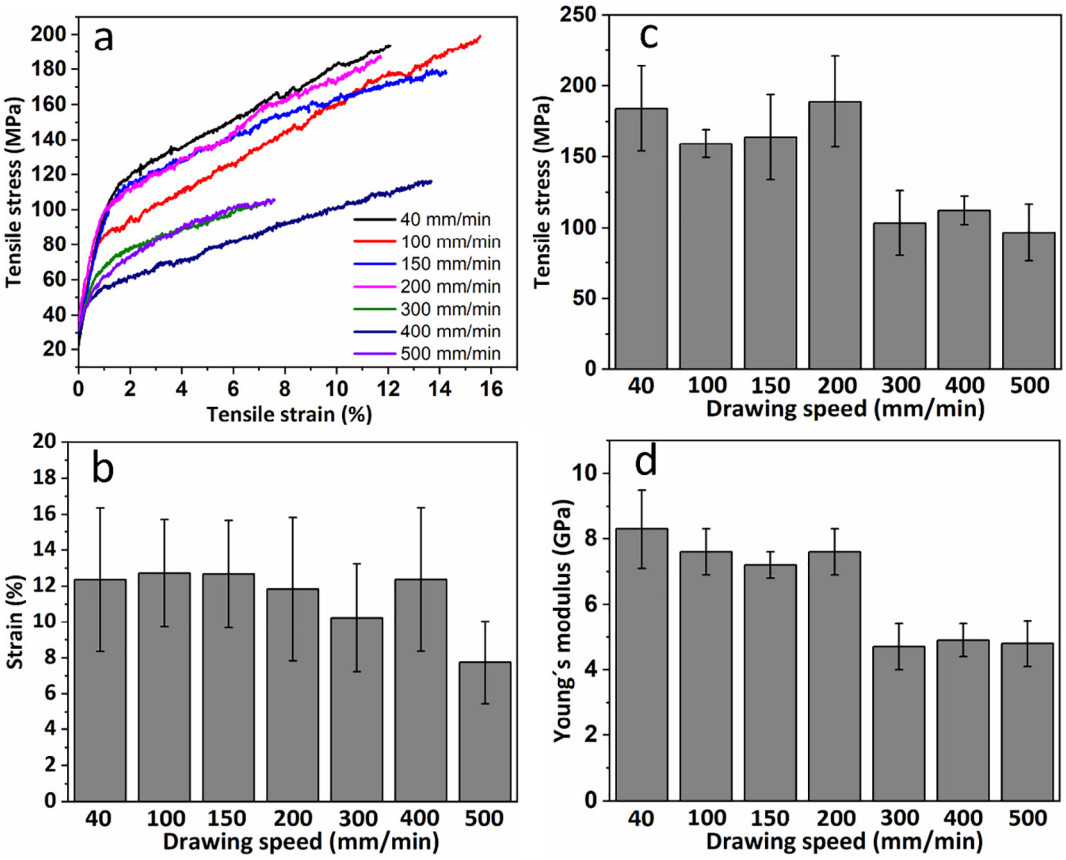

Fig. 2. Tensile properties of the TO-CNF/ChNC filaments fabricated using different drawing speed: (a) typical stress-strain curves, (b) strain at the break, (c) tensile stress, and (d) Young's modulus.

at 1580 cm^{-1} in ChNC shifted to 1552 cm^{-1}. All these changes in the DRIFT spectra of the TO-CNF/ChNC filament likely indicated the formation of ionic bonds between the carboxylate group of TO-CNF and the ammonium group of ChNC.

The TO-CNF/ChNC filament fabricated using 0.3 wt% ChNC and 0.3 wt% TO-CNF suspensions was further investigated via elemental analysis. The ChNC content in the TO-CNF/ChNC filament was calculated to be 47.6% by dividing the N content in the TO-CNF/ChNC filament by the N content in ChNC. We also calculated the theoretical value of ChNC in the TO-CNF/ChNC filament by dividing the theoretically absorbed ChNC weight by the theoretical total weight of TO-CNF/ChNC filament based on the charge ratio of cationic and anionic group contents of TO-CNF and ChNC (i.e., 1.7 g of 1.53 mmol/g TO-CNF assembled with 1.53 g of 1.7 mmol/g ChNC). The calculated theoretical content of ChNC in the TO-CNF/ChNC filament was 48%, which is close to the obtained experimental value (47.6%). This result suggests that the charges on the surface of ChNC and TO-CNF were almost fully compensated in the INC.

3.5. SEM images of TO-CNF/ChNC composite filaments

Fig. 4a shows an SEM image of a knot tied by the TO-CNF/ChNC filament, indicating good flexibility of the filaments. The TO-CNF/ChNC filament displayed a fibrous meridian structure, in which aligned

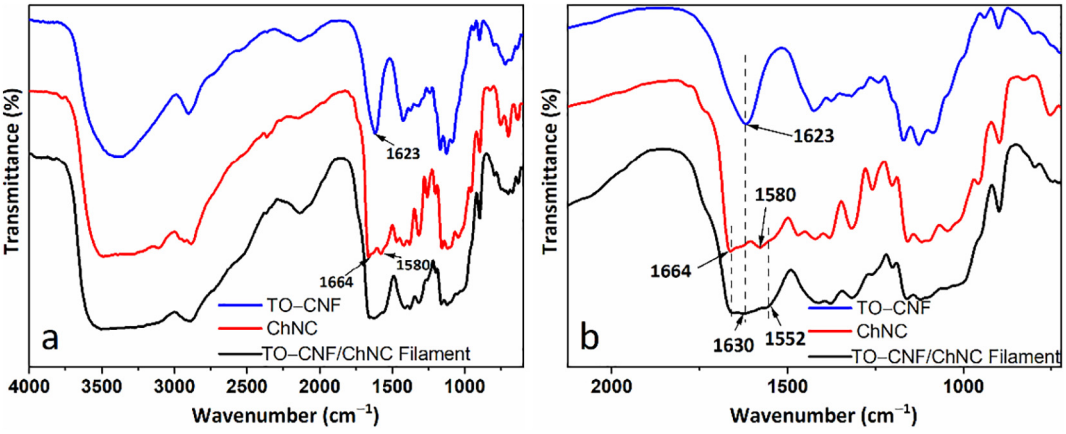

Fig. 3. (a) DRIFT spectra and (b) magnified DRIFT spectra of TO-CNF, ChNC and TO-CNF/ChNC filaments.

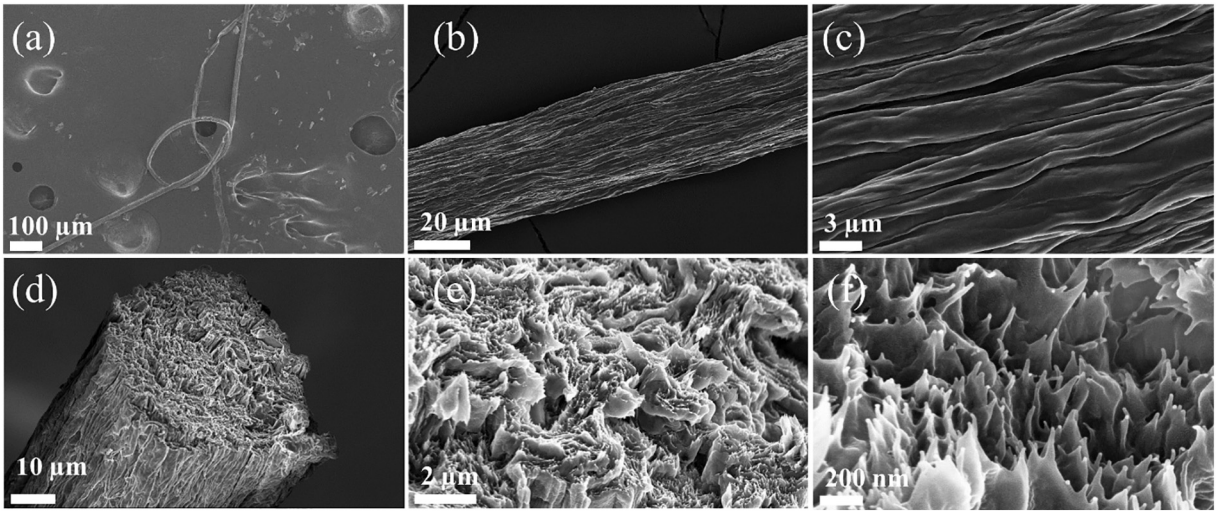

Fig. 4. Scanning electron microscopy (SEM) images of the (a–c) longitudinal direction and (d–f) cross-sectional fracture of TO-CNF/ChNC filament fabricated by 0.3 wt% TO-CNF and 0.3 wt % ChNC.

microscale fibers with diameters of 1–3 μm could be clearly observed in Fig. 4b and c, showing a similar hierarchical structure with previously reported pure nanocellulose INC filaments [51]. Obviously, a large number of nanofibers with an average diameter (10 ± 2 nm) larger than that of ChNC (6 ± 3 nm) or TO-CNF (5 ± 2 nm) could be found in the cross-section area. These nanofibers were assumed to be formed by the ionic combination of ChNCs and TO-CNF (more SEM images of TO-CNF/ChNC composite filaments can be found in Fig. S4 in Supplementary Information) [51].

3.6. Characterization of SWCNT@TO-CNF/ChNC filaments

Previously, NC has been used as an efficient surfactant to disperse CNTs (single- or multi-walled CNTs) to form aqueous suspensions with good stability [54]. Various types of CNT/NC composites, such as nanopaper, foams and fibers, have been fabricated based on this strategy [55]. Accordingly, we used TO-CNF to disperse SWCNTs and the obtained 0.3 wt% TO-CNF dispersion with 0.05, 0.1 or 0.2 wt% SWCNTs was used as an anionic component to draw TO-CNF/ChNC filament containing SWCNT (SWCNT@TO-CNF/ChNC filaments). 0.3 wt% TO-CNF suspensions with higher SWCNT concentrations were not considered because they cannot form filaments with 0.3 wt% ChNC; this is probably due to their high viscosity. The particle size of TO-CNF suspensions with various amount of SWCNT after sonication could be found in Fig. S5 in Supplementary information. TO-CNF with 0.05 and 0.1 wt% SWCNTs displayed a similar average diameter (about 1 μm). The average diameter of TO-CNF with 0.2 wt% SWCNTs was about 3 μm. All the obtained suspensions could stay stable for several months without phase separation (Fig. S6). Fig. 5 presents the morphologies of the formed SWCNT@TO-CNF/ChNC filaments. Like the neat TO-CNF/ChNC filament without CNTs, a typical fibrous structure could also be observed on the surface of the SWCNT@TO-CNF/ChNC filament. However, the SWCNT@TO-CNF/ChNC filament exhibited a rougher surface than the TO-CNF/ChNC filament. Moreover, a less dense and more irregular structure was observed in the fracture surface compared to TO-CNF/ChNC filament. The long and individualized SWCNTs were clearly recognizable in the cross-sectional area, different from the short nanofibers observed in the TO-CNF/ChNC filament, indicating the successful incorporation of the SWCNTs. Nevertheless, the short nanofibers observed in the TO-CNF/ChNC filament could not be found. Besides, the SWCNTs seems randomly arranged without orientation in the drawing direction.

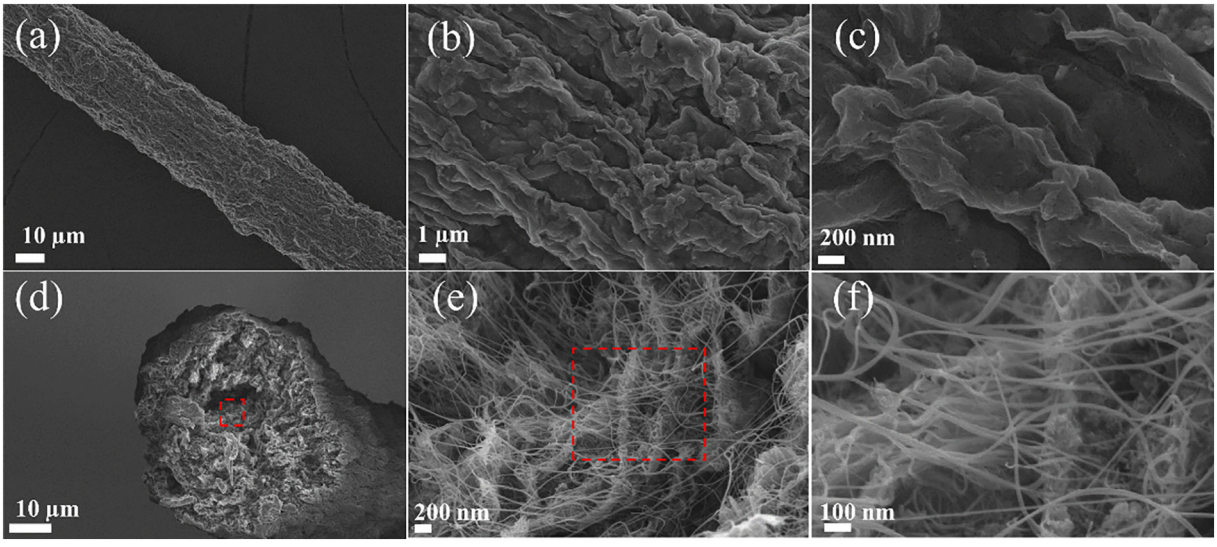

Fig. 5. SEM images in (a–c) longitudinal direction and (d–f) cross-sectional fracture of SWCNT@TO-CNF/ChNC filaments fabricated by 0.3 wt% ChNC and 0.3 wt% TO-CNF with 0.2 wt% SWCNTs.

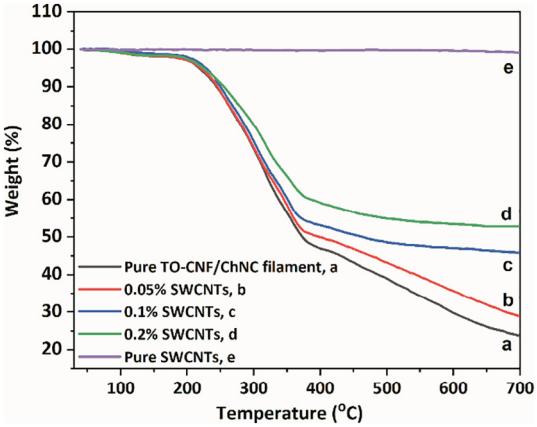

Fig. 6. TGA of (a–d) the TO-CNF/ChNC filament and the SWCNT@TO-CNF/ChNC filament fabricated with different CNT concentrations and of (e) pure SWCNTs.

Fig. 6 shows the TGA results of pure CNT and ChNCs/TO-CNF filaments fabricated using different concentrations of SWCNTs. All the samples showed an initial weight loss of between 35 and 100 °C due to the evaporation of absorbed moisture in the materials [73]. The pure TO-CNF/ChNC filament showed a major weight loss in the temperature range of 200–380 °C, which mainly came from the thermal degradation of cellulose and chitin [74,75]. Above 700 °C, the residual mass increased with increasing concentration of SWCNTs. The weight loss of pure SWCNTs was only 1% at temperatures up to 700 °C. On the basis of the residual mass at 700 °C, the percentage of nanotubes by weight was estimated. It was calculated that the content of SWCNTs in the SWCNT@TO-CNF/ChNC filaments fabricated from suspension containing 0.05, 0.1 and 0.2 wt% SWCNTs was 6.9, 29.3, and 38.6%, respectively. The SWCNT@TO-CNF/ChNC filament fabricated from 0.1 wt% SWCNTs showed a much higher CNTs content (about four times) than the filament obtained from 0.05 wt% SWCNTs. We believe that the amount of incorporated CNTs into the filament was quite related to the formation mechanism of the filaments with CNTs. TO-CNF was used as "surfactant" to disperse CNTs, in which TO-CNF and CNTs could interact with each other and form electrostatically stabilized associated structures [54]. Then, these associated structures would assemble with cationic ChNC to form the filament [76]. Thus, the content of CNTs in the formed filaments is depended not only on the association between TO-CNF and CNTs but also on the electrostatic interaction between the associated structures and ChNC. With 0.3 wt% TO-CNF, both 0.05 wt% and 0.1 wt % CNTs could be dispersed well (average diameter is about 1 μm). Thus, for 0.3 wt% TO-CNF suspension with 0.05 wt% CNTs, there are probably more TO-CNFs associated with CNTs. In turn, more ChNC will be incorporated into formed filament, resulting in a relatively lower content of CNTs compared to that of filament formed by 0.3 wt% TO-CNF with 0.1 wt% CNTs. The quantitative calculation of the amount of TO-CNF interacted with CNTs is still unclear [54], which needs more investigations in future.

Fig. 7 and Table 2 present the mechanical and electrical properties of the SWCNT@TO-CNF/ChNC filaments. The addition of the SWCNTs exhibited a negative effect on the mechanical properties, i.e., the tensile strength, strain, and Young's modulus of the SWCNT@TO-CNF/ChNC filaments decreased compared to those of the TO-CNF/ChNC filament. It is likely that the SWCNTs led to insufficient complexation between ChNC and TO-CNF and a less homogeneous structure than the TO-CNF/ChNC filament. The strain was also decreased due to the rigidity of SWCNTs [77]. With the increase of SWCNT concentration from 0.1 to 0.2 wt%, SWCNTs@TO-CNF/ChNC filaments showed a similar tensile strength and Young's modulus. This might be explained by the fact that with the higher SWCNT content embedded inside the fiber, the SWCNT network compensated for the loose structure of the filament and provided structural integrity and mechanical strength to the filaments [78]. The electrical properties of the SWCNT@TO-CNF/ChNC filaments were measured using a two-point probe. All the SWCNT@TO-CNF/ChNC filaments displayed linear *I–V* curves, revealing an Ohmic behavior. Notably, the conductivity of the filaments improved dramatically with increasing SWCNT content in the original dispersion. The electrical conductivity of the filament fabricated by 0.2% SWCNTs was 2056 S/m. The formed SWCNTs@TO-CNF/ChNC filament showed a comparable mechanical and electrical conductivity to the previous report based on similar strategy i.e., polyelectrolyte complexation. For example, Granero et al. [77] used the wet-spinning method to inject SWCNTs (dispersing in carrageenan) into oppositely charged chitosan based on IPC, resulting in a conductive fiber with a conductivity of 20.6 S/cm and a tensile strength of 104 MPa. However, the tensile strength is still lower than that of SWCNTs/TO-CNF hybrid fibers prepared via traditional wet-spinning (260–472 MPa) or 3D-printing method (~247 MPa) [60,62]. Therefore, in order to improve the strength of INC fibers, further investigations, for example, the effects of stretching or alignment of nanofiber, need to be conducted in future.

4. Conclusion

In this study, the drawing of composite filaments based on oppositely charged nanoparticles (anionic TO-CNF and cationic ChNC), using interfacial nanoparticle complexation (INC) was demonstrated. By increasing the drawing speed, the mechanical properties of the TO-CNF/ChNC filaments decreased, exhibiting a phenomenon opposite to that of traditional wet-spinning. A relatively slow drawing speed is required for the INC method in order to offer enough time for the

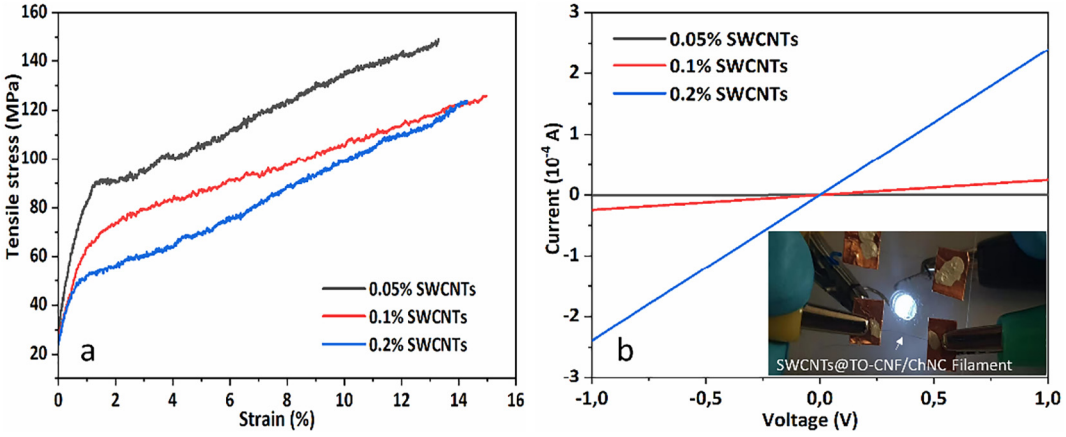

Fig. 7. Typical strain–stress curves (a) and I–V curves (e) of the SWCNT@TO-CNF/ChNC filaments fabricated with different CNT concentrations; the inset in part (b) is the formed filament used as a conductive line to light an LED.

Table 2
Characteristics of the fabricated SWCNT@TO-CNF/ChNC filaments.

Sample[a]	SWCNTs content (%)	Ultimate tensile strength (MPa)	Strain at break (%)	Young's modulus (GPa)	Electrical conductivity (S/m)
0% SWCNTs	–	184 ± 20	12.3 ± 4	8.9 ± 2	–
0.05% SWCNTs	6.9	149 ± 17	12.6 ± 2	7.3 ± 3	9.6 ± 3
0.1% SWCNTs	29.3	121 ± 11	11.6 ± 3	6.0 ± 2	388 ± 60
0.2% SWCNTs	38.6	125 ± 13	10.5 ± 3	6.3 ± 2	2056 ± 230

[a] Filament prepared from 0.3 wt% TO-CNFs and 0.3 wt% ChNCs with different SWCNTs concentration.

interfacial complexation of two oppositely charged nanoparticles. With a drawing speed of 40 mm/min, a TO-CNF/ChNC filament with a tensile strength of 184 MPa and Young's modulus of 8.3 GPa were obtained. Moreover, SWCNTs were successfully incorporated into TO-CNF/ChNC filaments. Even though mechanical properties decreased, conductive filaments with a tensile strength of and an electrical conductivity of 2056 S/m were obtained.

Supplementary data to this article can be found online at https://doi.org/10.1016/j.matdes.2020.108594.

CRediT authorship contribution statement

Kaitao Zhang: Conceptualization, Methodology, Writing - original draft, Formal analysis. **Lukas Ketterle:** Formal analysis, Investigation. **Topias Järvinen:** Formal analysis, Investigation. **Shu Hong:** Formal analysis. **Henrikki Liimatainen:** Writing - review & editing, Project administration, Funding acquisition, Supervision.

Declaration of competing interest

The authors declare that they have no known competing financial interests or personal relationships that could have appeared to influence the work reported in this paper.

Acknowledgements

The authors acknowledge the support from the Academy of Finland project "Bionanochemicals" (298295) and European Regional Development Fund/Council of Oulu Region ("Novidam" project), Finland. We also thank the support of Center of Microscopy and Nanotechnology in University of Oulu, Elisa Wirkkala for technical assistance in elemental analysis.

Data availability

All data needed to evaluate the conclusions in the paper are present in the paper and/or the Supplementary Materials. The raw/processed data required to reproduce these findings can be shared from the corresponding authors upon reasonable requests.

References

[1] A.G. Cunha, A. Gandini, Turning polysaccharides into hydrophobic materials: a critical review. Part 1. Cellulose, Cellulose 17 (5) (2010) 875–889.
[2] N. Lin, J. Huang, A. Dufresne, Preparation, properties and applications of polysaccharide nanocrystals in advanced functional nanomaterials: a review, Nanoscale 4 (11) (2012) 3274–3294.
[3] D. Trache, M.H. Hussin, M.K.M. Haafiz, V.K. Thakur, Recent progress in cellulose nanocrystals: sources and production, Nanoscale 9 (5) (2017) 1763–1786.
[4] H. Liimatainen, M. Visanko, J. Sirviö, O. Hormi, J. Niinimäki, Sulfonated cellulose nanofibrils obtained from wood pulp through regioselective oxidative bisulfite pre-treatment, Cellulose 20 (2) (2013) 741–749.
[5] J.A. Sirviö, T. Hasa, J. Ahola, H. Liimatainen, J. Niinimäki, O. Hormi, Phosphonated nanocelluloses from sequential oxidative-reductive treatment - physicochemical characteristics and thermal properties, Carbohyd Polym 133 (2015) 524–532.
[6] J.A. Sirvio, M.T. Visanko, Anionic wood nanofibers produced from unbleached mechanical pulp by highly efficient chemical modification, J. Mater. Chem. A 5 (40) (2017) 21828–21835.
[7] J.A. Sirviö, J. Ukkola, H. Liimatainen, Direct sulfation of cellulose fibers using a reactive deep eutectic solvent to produce highly charged cellulose nanofibers, Cellulose 26 (4) (2019) 2303–2316.
[8] T. Selkälä, J.A. Sirviö, G.S. Lorite, H. Liimatainen, Anionically stabilized cellulose nanofibrils through succinylation pretreatment in urea–lithium chloride deep eutectic solvent, Chemsuschem 9 (21) (2016) 3074–3083.
[9] H.P.S. Abdul Khalil, Y. Davoudpour, M.N. Islam, A. Mustapha, K. Sudesh, R. Dungani, M. Jawaid, Production and modification of nanofibrillated cellulose using various mechanical processes: a review, Carbohyd Polym 99 (Supplement C) (2014) 649–665.
[10] P. Li, J.A. Sirviö, A. Haapala, H. Liimatainen, Cellulose nanofibrils from nonderivatizing urea-based deep eutectic solvent pretreatments, ACS Appl. Mater. Interfaces 9 (3) (2017) 2846–2855.
[11] I.A. Sacui, R.C. Nieuwendaal, D.J. Burnett, S.J. Stranick, M. Jorfi, C. Weder, E.J. Foster, R.T. Olsson, J.W. Gilman, Comparison of the properties of cellulose nanocrystals and cellulose nanofibrils isolated from bacteria, tunicate, and wood processed using acid, enzymatic, mechanical, and oxidative methods, Acs Appl Mater Inter 6 (9) (2014) 6127–6138.
[12] S. Ifuku, Chitin and chitosan nanofibers: preparation and chemical modifications, Molecules 19 (11) (2014) 18367–18380.
[13] B. Duan, Y. Huang, A. Lu, L. Zhang, Recent advances in chitin based materials constructed via physical methods, Prog. Polym. Sci. 82 (2018) 1–33.
[14] A.M. Salaberria, S.C.M. Fernandes, R.H. Diaz, J. Labidi, Processing of α-chitin nanofibers by dynamic high pressure homogenization: characterization and antifungal activity against A. niger, Carbohyd Polym 116 (2015) 286–291.
[15] S. Hong, Y. Yuan, Q. Yang, L. Chen, J. Deng, W. Chen, H. Lian, J.D. Mota-Morales, H. Liimatainen, Choline chloride-zinc chloride deep eutectic solvent mediated preparation of partial O-acetylation of chitin nanocrystal in one step reaction, Carbohyd Polym 220 (2019) 211–218.
[16] W. Ye, H. Ma, L. Liu, J. Yu, J. Lai, Y. Fang, Y. Fan, Biocatalyzed route for the preparation of surface-deacetylated chitin nanofibers, Green Chem. 21 (11) (2019) 3143–3151.
[17] Y. Fan, T. Saito, A. Isogai, TEMPO-mediated oxidation of β-chitin to prepare individual nanofibrils, Carbohyd Polym 77 (4) (2009) 832–838.
[18] J.-B. Zeng, Y.-S. He, S.-L. Li, Y.-Z. Wang, Chitin whiskers: an overview, Biomacromolecules 13 (1) (2012) 1–11.
[19] D. Klemm, E.D. Cranston, D. Fischer, M. Gama, S.A. Kedzior, D. Kralisch, F. Kramer, T. Kondo, T. Lindström, S. Nietzsche, K. Petzold-Welcke, F. Rauchfuß, Nanocellulose as a natural source for groundbreaking applications in materials science: today's state, Mater. Today 21 (7) (2018) 720–748.
[20] S.J. Eichhorn, Cellulose nanowhiskers: promising materials for advanced applications, Soft Matter 7 (2) (2011) 303–315.
[21] E.J. Foster, R.J. Moon, U.P. Agarwal, M.J. Bortner, J. Bras, S. Camarero-Espinosa, K.J. Chan, M.J.D. Clift, E.D. Cranston, S.J. Eichhorn, D.M. Fox, W.Y. Hamad, L. Heux, B. Jean, M. Korey, W. Nieh, K.J. Ong, M.S. Reid, S. Renneckar, R. Roberts, J.A. Shatkin, J. Simonsen, K. Stinson-Bagby, N. Wanasekara, J. Youngblood, Current characterization methods for cellulose nanomaterials, Chem. Soc. Rev. 47 (8) (2018) 2609–2679.
[22] S. Ifuku, H. Saimoto, Chitin nanofibers: preparations, modifications, and applications, Nanoscale 4 (11) (2012) 3308–3318.
[23] N. Mohammed, N. Grishkewich, K.C. Tam, Cellulose nanomaterials: promising sustainable nanomaterials for application in water/wastewater treatment processes, Environmental Science: Nano 5 (3) (2018) 623–658.
[24] Y. Xue, Z. Mou, H. Xiao, Nanocellulose as a sustainable biomass material: structure, properties, present status and future prospects in biomedical applications, Nanoscale 9 (39) (2017) 14758–14781.
[25] R. Jayakumar, M. Prabaharan, S.V. Nair, H. Tamura, Novel chitin and chitosan nanofibers in biomedical applications, Biotechnol. Adv. 28 (1) (2010) 142–150.
[26] Y. Liu, F. Wu, X. Zhao, M. Liu, High-performance strain sensors based on spirally structured composites with carbon black, chitin nanocrystals, and natural rubber, ACS Sustain. Chem. Eng. 6 (8) (2018) 10595–10605.
[27] L. Bai, S. Huan, W. Xiang, L. Liu, Y. Yang, R.W.N. Nugroho, Y. Fan, O.J. Rojas, Self-assembled networks of short and long chitin nanoparticles for oil/water interfacial superstabilization, ACS Sustain. Chem. Eng. 7 (7) (2019) 6497–6511.
[28] P. Ang-atikarnkul, A. Watthanaphanit, R. Rujiravanit, Fabrication of cellulose nanofiber/chitin whisker/silk sericin bionanocomposite sponges and characterizations of their physical and biological properties, Compos. Sci. Technol. 96 (2014) 88–96.
[29] E. Kontturi, P. Laaksonen, M.B. Linder, Nonappa, A.H. Groschel, O.J. Rojas, O. Ikkala, Advanced materials through assembly of nanocelluloses, Adv. Mater. 30 (24) (2018), e1703779.
[30] M.J. Lundahl, V. Klar, L. Wang, M. Ago, O.J. Rojas, Spinning of cellulose nanofibrils into filaments: a review, Ind. Eng. Chem. Res. 56 (1) (2017) 8–19.
[31] H. Liimatainen, N. Ezekiel, R. Sliz, K. Ohenoja, J.A. Sirviö, L. Berglund, O. Hormi, J. Niinimäki, High-strength nanocellulose-talc hybrid barrier films, ACS Appl. Mater. Interfaces 5 (24) (2013) 13412–13418.

[32] J.A. Sirviö, S. Honkaniemi, M. Visanko, H. Liimatainen, Composite films of poly(vinyl alcohol) and bifunctional cross-linking cellulose nanocrystals, ACS Appl. Mater. Interfaces 7 (35) (2015) 19691–19699.
[33] Y. Fan, H. Fukuzumi, T. Saito, A. Isogai, Comparative characterization of aqueous dispersions and cast films of different chitin nanowhiskers/nanofibers, Int. J. Biol. Macromol. 50 (1) (2012) 69–76.
[34] W.M. Fazli Wan Nawawi, K.-Y. Lee, E. Kontturi, R.J. Murphy, A. Bismarck, Chitin nanopaper from mushroom extract: natural composite of nanofibers and glucan from a single biobased source, ACS Sustain. Chem. Eng. 7 (7) (2019) 6492–6496.
[35] L. Heath, L. Zhu, W. Thielemans, Chitin nanowhisker aerogels, Chemsuschem 6 (3) (2013) 537–544.
[36] C. Chen, D. Li, H. Yano, K. Abe, Bioinspired hydrogels: Quinone crosslinking reaction for chitin nanofibers with enhanced mechanical strength via surface deacetylation, Carbohyd Polym 207 (2019) 411–417.
[37] P. Mohammadi, A.S. Aranko, C.P. Landowski, O. Ikkala, K. Jaudzems, W. Wagermaier, M.B. Linder, Biomimetic composites with enhanced toughening using silk-inspired triblock proteins and aligned nanocellulose reinforcements, Sci. Adv. 5 (9) (2019) eaaw2541.
[38] S. Hooshmand, Y. Aitomäki, L. Berglund, A.P. Mathew, K. Oksman, Enhanced alignment and mechanical properties through the use of hydroxyethyl cellulose in solvent-free native cellulose spun filaments, Compos. Sci. Technol. 150 (2017) 79–86.
[39] L. Geng, B. Chen, X. Peng, T. Kuang, Strength and modulus improvement of wet-spun cellulose I filaments by sequential physical and chemical cross-linking, Mater. Des. 136 (2017) 45–53.
[40] M. Karzar Jeddi, O. Laitinen, H. Liimatainen, Magnetic superabsorbents based on nanocellulose aerobeads for selective removal of oils and organic solvents, Mater. Des. 183 (2019), 108115.
[41] X. Zhang, I. Elsayed, C. Navarathna, G. Schueneman, E.B. Hassan, Biohybrid hydrogel and aerogel from self-assembled nanocellulose and nanochitin as a high-efficiency adsorbent for water purification, Acs Appl Mater Inter 11 (50) (2019) 46714–46725.
[42] A. Poskela, K. Miettunen, M. Borghei, J. Vapaavuori, L.G. Greca, J. Lehtonen, K. Solin, M. Ago, P.D. Lund, O.J. Rojas, Nanocellulose and nanochitin cryogels improve the efficiency of dye solar cells, ACS Sustain. Chem. Eng. 7 (12) (2019) 10257–10265.
[43] C.C. Satam, C.W. Irvin, C.J. Coffey, R.K. Geran, R. Ibarra-Rivera, M.L. Shofner, J.C. Meredith, Controlling barrier and mechanical properties of cellulose nanocrystals by blending with chitin nanofibers, Biomacromolecules 21 (2) (2020) 545–555.
[44] Z.D. Qi, T. Saito, Y. Fan, A. Isogai, Multifunctional coating films by layer-by-layer deposition of cellulose and chitin nanofibrils, Biomacromolecules 13 (2) (2012) 553–558.
[45] T. Kim, T.H. Tran, S.Y. Hwang, J. Park, D.X. Oh, B.-S. Kim, Crab-on-a-tree: all biorenewable, optical and radio frequency transparent barrier nanocoating for food packaging, ACS Nano 13 (4) (2019) 3796–3805.
[46] M.S. Toivonen, S. Kurki-Suonio, W. Wagermaier, V. Hynninen, S. Hietala, O. Ikkala, Interfacial polyelectrolyte complex spinning of cellulose nanofibrils for advanced bicomponent fibers, Biomacromolecules 18 (4) (2017) 1293–1301.
[47] R. Grande, E. Trovatti, A.J.F. Carvalho, A. Gandini, Continuous microfiber drawing by interfacial charge complexation between anionic cellulose nanofibers and cationic chitosan, J. Mater. Chem. A 5 (25) (2017) 13098–13103.
[48] A.C.A. Wan, M.F.A. Cutiongco, B.C.U. Tai, M.F. Leong, H.F. Lu, E.K.F. Yim, Fibers by interfacial polyelectrolyte complexation – processes, materials and applications, Mater. Today 19 (8) (2016) 437–450.
[49] M. Do, B.G. Im, J.P. Park, J.-H. Jang, H. Lee, Functional polysaccharide sutures prepared by wet fusion of interfacial polyelectrolyte complexation fibers, Adv. Funct. Mater. 27 (42) (2017) 1702017(n/a).
[50] B.C.U. Tai, A.C.A. Wan, J.Y. Ying, Modified polyelectrolyte complex fibrous scaffold as a matrix for 3D cell culture, Biomaterials 31 (23) (2010) 5927–5935.
[51] K. Zhang, H. Liimatainen, Hierarchical assembly of nanocellulose-based filaments by interfacial complexation, Small 14 (38) (2018) 1801937.
[52] R. Grande, L. Bai, L. Wang, W. Xiang, O. Ikkala, A.J.F. Carvalho, O.J. Rojas, Nanochitins of varying aspect ratio and properties of microfibers produced by interfacial complexation with seaweed alginate, ACS Sustain. Chem. Eng. 8 (2) (2019) 1137–1145.
[53] J.M. González-Domínguez, A. Ansón-Casaos, L. Grasa, L. Abenia, A. Salvador, E. Colom, J.E. Mesonero, J.E. García-Bordejé, A.M. Benito, W.K. Maser, Unique properties and behavior of nonmercerized type-II cellulose nanocrystals as carbon nanotube biocompatible dispersants, Biomacromolecules 20 (8) (2019) 3147–3160.
[54] A. Hajian, S.B. Lindström, T. Pettersson, M.M. Hamedi, L. Wågberg, Understanding the dispersive action of nanocellulose for carbon nanomaterials, Nano Lett. 17 (3) (2017) 1439–1447.
[55] M.M. Hamedi, A. Hajian, A.B. Fall, K. Håkansson, M. Salajkova, F. Lundell, L. Wågberg, L.A. Berglund, Highly conducting, strong nanocomposites based on nanocellulose-assisted aqueous dispersions of single-wall carbon nanotubes, ACS Nano 8 (3) (2014) 2467–2476.
[56] C. Olivier, C. Moreau, P. Bertoncini, H. Bizot, O. Chauvet, B. Cathala, Cellulose nanocrystal-assisted dispersion of luminescent single-walled carbon nanotubes for layer-by-layer assembled hybrid thin films, Langmuir 28 (34) (2012) 12463–12471.
[57] M. Wang, I.V. Anoshkin, A.G. Nasibulin, R.H.A. Ras, Nonappa, J. Laine, E.I. Kauppinen, O. Ikkala, Electrical behaviour of native cellulose nanofibril/carbon nanotube hybrid aerogels under cyclic compression, RSC Adv. 6 (92) (2016) 89051–89056.
[58] Q. Zheng, Z. Cai, Z. Ma, S. Gong, Cellulose nanofibril/reduced graphene oxide/carbon nanotube hybrid aerogels for highly flexible and all-solid-state supercapacitors, Acs Appl Mater Inter 7 (5) (2015) 3263–3271.
[59] J. Han, H. Wang, Y. Yue, C. Mei, J. Chen, C. Huang, Q. Wu, X. Xu, A self-healable and highly flexible supercapacitor integrated by dynamically cross-linked electroconductive hydrogels based on nanocellulose-templated carbon nanotubes embedded in a viscoelastic polymer network, Carbon 149 (2019) 1–18.
[60] S.-Y. Cho, H. Yu, J. Choi, H. Kang, S. Park, J.-S. Jang, H.-J. Hong, I.-D. Kim, S.-K. Lee, H.S. Jeong, H.-T. Jung, Continuous meter-scale synthesis of weavable tunicate cellulose/carbon nanotube fibers for high-performance wearable sensors, ACS Nano 13 (8) (2019) 9332–9341.
[61] Y. Li, H. Zhu, Y. Wang, U. Ray, S. Zhu, J. Dai, C. Chen, K. Fu, S.-H. Jang, D. Henderson, T. Li, L. Hu, Cellulose-nanofiber-enabled 3D printing of a carbon-nanotube microfiber network, Small Methods 1 (10) (2017) 1700222(n/a).
[62] Z. Wan, C. Chen, T. Meng, M. Mojtaba, Y. Teng, Q. Feng, D. Li, Multifunctional wet-spun filaments through robust nanocellulose networks wrapping to single-walled carbon nanotubes, Acs Appl Mater Inter 11 (45) (2019) 42808–42817.
[63] K. Zhang, P. Sun, H. Liu, S. Shang, J. Song, D. Wang, Extraction and comparison of carboxylated cellulose nanocrystals from bleached sugarcane bagasse pulp using two different oxidation methods, Carbohyd Polym 138 (2016) 237–243.
[64] T. Saito, A. Isogai, TEMPO-mediated oxidation of native cellulose. The effect of oxidation conditions on chemical and crystal structures of the water-insoluble fractions, Biomacromolecules 5 (5) (2004) 1983–1989.
[65] Y. Fan, T. Saito, A. Isogai, Individual chitin nano-whiskers prepared from partially deacetylated α-chitin by fibril surface cationization, Carbohyd Polym 79 (4) (2010) 1046–1051.
[66] T. Suopajärvi, J.A. Sirviö, H. Liimatainen, Cationic nanocelluloses in dewatering of municipal activated sludge, Journal of Environmental Chemical Engineering 5 (1) (2017) 86–92.
[67] A.C.A. Wan, E.K.F. Yim, I.C. Liao, C. Le Visage, K.W. Leong, Encapsulation of biologics in self-assembled fibers as biostructural units for tissue engineering, J. Biomed. Mater. Res. A 71A (4) (2004) 586–595.
[68] T. Saito, S. Kimura, Y. Nishiyama, A. Isogai, Cellulose nanofibers prepared by TEMPO-mediated oxidation of native cellulose, Biomacromolecules 8 (8) (2007) 2485–2491.
[69] L. Liu, R. Wang, J. Yu, J. Jiang, K. Zheng, L. Hu, Z. Wang, Y. Fan, Robust self-standing chitin nanofiber/nanowhisker hydrogels with designed surface charges and ultralow mass content via gas phase coagulation, Biomacromolecules 17 (11) (2016) 3773–3781.
[70] J. Ostrowska-Czubenko, M. Gierszewska-Drużyńska, Effect of ionic crosslinking on the water state in hydrogel chitosan membranes, Carbohyd Polym 77 (3) (2009) 590–598.
[71] R.S. Rabelo, G.M. Tavares, A.S. Prata, M.D. Hubinger, Complexation of chitosan with gum Arabic, sodium alginate and κ-carrageenan: effects of pH, polymer ratio and salt concentration, Carbohyd Polym 223 (2019), 115120.
[72] K. Chi, J.M. Catchmark, Improved eco-friendly barrier materials based on crystalline nanocellulose/chitosan/carboxymethyl cellulose polyelectrolyte complexes, Food Hydrocolloid 80 (2018) 195–205.
[73] A.T. Paulino, J.I. Simionato, J.C. Garcia, J. Nozaki, Characterization of chitosan and chitin produced from silkworm crysalides, Carbohyd Polym 64 (1) (2006) 98–103.
[74] N. Johar, I. Ahmad, A. Dufresne, Extraction, preparation and characterization of cellulose fibres and nanocrystals from rice husk, Ind. Crop. Prod. 37 (1) (2012) 93–99.
[75] H.Z. Zou, B.F. Lin, C.H. Xu, M.J. Lin, W. Zhan, Preparation and characterization of individual chitin nanofibers with high stability from chitin gels by low-intensity ultrasonication for antibacterial finishing, Cellulose 25 (2) (2018) 999–1010.
[76] K. Zhang, S.D. Hujaya, T. Jarvinen, P. Li, T. Kauhanen, M.V. Tejesvi, K. Kordas, H. Liimatainen, Interfacial nanoparticle complexation of oppositely charged nanocelluloses into functional filaments with conductive, drug release, or antimicrobial property, ACS Appl. Mater. Interfaces 12 (1) (2020) 1765–1774.
[77] A.J. Granero, J.M. Razal, G.G. Wallace, M. in het Panhuis, Conducting gel-fibres based on carrageenan, chitosan and carbon nanotubes, J. Mater. Chem. 20 (37) (2010) 7953–7956.
[78] S. Razdan, P.K. Patra, S. Kar, L. Ci, R. Vajtai, Á. Kukovecz, Z. Kónya, I. Kiricsi, P.M. Ajayan, Ionically self-assembled polyelectrolyte-based carbon nanotube fibers, Chem. Mater. 21 (14) (2009) 3062–3071.